IEEE Access
Multidisciplinary | Rapid Review | Open Access Journal

Received September 15, 2021, accepted October 29, 2021, date of publication November 4, 2021,
date of current version November 11, 2021.

Digital Object Identifier 10.1109/ACCESS.2021.3125522

A High-Performance Isolated SEPIC Converter for Non-Electrolytic LED Lighting

SULAIHA AHMAD[1], NADIA MEI LIN TAN[2,3], (Senior Member, IEEE), M. ZAFRI BAHARUDDIN[4], (Member, IEEE), AND GIAMPAOLO BUTICCHI[2], (Senior Member, IEEE)

[1]Institute of Energy Policy and Research (IEPRe), Universiti Tenaga Nasional, Kajang, Selangor 43000, Malaysia
[2]Zhejiang Key Laboratory on the More Electric Aircraft Technologies, University of Nottingham Ningbo China, Ningbo 315100, China
[3]Institute of Power Engineering, Universiti Tenaga Nasional, Kajang, Selangor 43000, Malaysia
[4]Department of Electrical and Electronics Engineering, College of Engineering, Universiti Tenaga Nasional, Kajang, Selangor 43000, Malaysia

Corresponding author: Nadia Mei Lin Tan (nadia.tan@nottingham.edu.cn)

This work was supported in part by the Universiti Tenaga Nasional BOLD2020 Grant under Project RJO10517844/110, and in part by the Ministry of Science and Technology through the National Key Research and Development Program of China under Grant 2021YFE0108600.

ABSTRACT This paper proposes a high-performance isolated single-ended primary inductor converter (SEPIC) that is integrated with a non-dissipative snubber for a light-emitting diode (LED) driver. The proposed LED driver employs the snubber circuit to minimize any switching overvoltage caused by parasitic leakage inductance of the high-frequency transformer in the isolated SEPIC converter. This paper also presents a detail theoretical analysis of the proposed LED driver including its operating modes and design calculation. The experimental results of the proposed LED driver at the rated power of 18 W shows that it has a high-power factor, low harmonics, employs non-electrolytic capacitors, low switching stress, high reliability and high efficiency.

INDEX TERMS Isolated SEPIC, LED driver, non-dissipative snubber, high efficiency, non-electrolytic capacitor.

I. INTRODUCTION

A light-emitting diode (LED) requires an LED driver to convert ac power to dc power. The LED driver is the likeliest to fail before the expected lifetime of the LED. Other causes of LED breakdown include housing, packaging and controller failures [1]. The risk of circuit failure in an LED driver may be caused by failure of electrolytic capacitor, switching overvoltage, and overcurrent.

A typical LED driver employs a line-frequency transformer in the circuit design to provide galvanic isolation. An indoor LED light with rated power of more than 15W and an outdoor LED light of any rated power will employ a line-frequency transformer to provide galvanic isolation in the driver [2].

In order to reduce the footprint of an LED driver, a high-frequency transformer is employed such as that in an isolated single-ended primary inductance converter (SEPIC) [3]–[5], flyback [6]–[8], push-pull [9], half-bridge [10], and full-bridge [11] converters. The flyback and SEPIC converters are simpler, more reliable and cost-effective compared to the other aforementioned converters because they use only one switch. However, the peak input current in flyback converter is high which increases the component's rating and cost. It also requires two different feedback controllers to solve the power factor and flicker issues [6]–[8]. On the other hand, SEPIC converter is able to achieve high power factor when its input inductor operates in discontinuous mode (DCM) operation which reduces the complexity and cost for a power factor correction (PFC) circuit.

Fig. 1(a) shows the topology of an LED driver that is based on a snubberless isolated SEPIC. The switching frequency of isolated SEPIC is typically more than 50 kHz and high-frequency transformer T_1 is employed. However, the leakage inductance L_{lk} in the high-frequency transformer T_1 causes overvoltage in the switch at every turn-off interval. Fig. 1(b) illustrates a 286 V overvoltage during switch turn-off in a practical 90 V ac-dc isolated SEPIC LED driver. The transient spike in switch voltage will increase switch voltage stress and switching loss in S_1. Therefore, a snubber circuit is required

The associate editor coordinating the review of this manuscript and approving it for publication was Amedeo Andreotti.

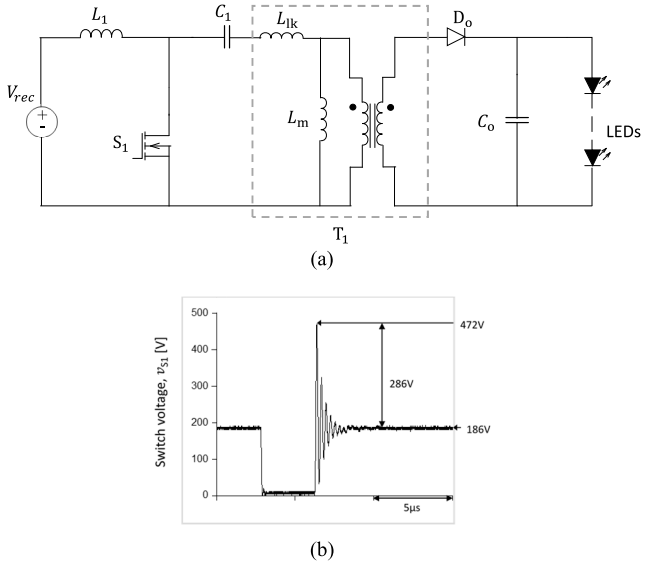

FIGURE 1. (a) Snubberless isolated SEPIC converter. (b) Switching overvoltage in an isolated SEPIC LED driver.

to minimise the overvoltage to improve the reliability of the LED driver.

There are two types of overvoltage snubbers which are the passive and active snubbers. The latter type of snubber reduces the switching overvoltage by using an active circuit controller. The typical advantage of an active snubber compared to the passive snubber is zero-voltage switching (ZVS) or zero-current switching (ZCS). However, more switches and controllers are required which increases the size, cost and complexity of the overall system. It also compromises the reliability of the circuit.

The conventional passive snubber is known as a resistor-capacitor-diode (RCD) snubber [12]. It is a low-cost and straightforward solution to reduce the switching overvoltage. However, the snubber loss is not negligible, thus reducing the efficiency of the LED driver. To prevent losses in RCD snubber, an inductor capacitor diode (LCD) snubber has been used. The Domb-Redl-Sokal (DRS) snubber is a common non-dissipative LCD snubber for a flyback converter [13]. Nevertheless, the application of a DRS in an ac-dc isolated SEPIC converter for LED lighting is not yet available in the literature.

This paper proposes an LED driver that is based on a high-performance isolated SEPIC that utilizes a non-dissipative DRS snubber [14]. The distinctive characteristics of the proposed LED driver are that it has a high-frequency transformer for isolation, minimised switch overvoltage, single-stage converter, high power factor and low harmonics. This paper also describes the topology of the proposed LED driver, its operating modes and design methodology. The simulation and experimental results validate that the proposed LED driver meets the strict requirements of a well-designed LED lighting system such as low harmonics, high power factor, high reliability and high efficiency.

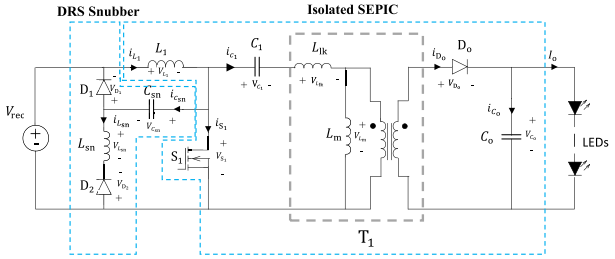

FIGURE 2. The proposed LED driver.

II. CIRCUIT DESCRIPTION

Fig. 2 shows the proposed LED driver that is based on a non-dissipative isolated SEPIC circuit. The dc input voltage V_{rec} is the rectified average voltage of a single-phase full-bridge uncontrolled rectifier. The isolated SEPIC consists of an input inductor L_1, a MOSFET switch S_1, a storage capacitor C_1, a high-frequency transformer T_1, an output diode D_o and an output capacitor C_o. A non-dissipative DRS snubber that consists of snubber capacitor C_{sn}, snubber inductor L_{sn} and snubber diodes D_1 and D_2 are employed with the isolated SEPIC to improve circuit reliability. In practice, the parasitic leakage inductance of T_1, L_{lk} will cause overvoltage across switch S_1 at every switch turn-off. The DRS snubber is used to clamp the overvoltage across S_1 to an acceptable level.

To ensure a near-unity power factor, the current in inductor L_1 is in DCM so that the ac current waveform matches the ac source voltage waveform [15]. In the proposed LED driver, a feedback controller is not required for power factor correction. Therefore, the overall size and complexity of the LED driver is reduced. Transformer T_1 has a turns-ratio of 1:1 and it galvanically isolates the primary and secondary side of the proposed LED driver, providing protection to the circuit and users in the case of short-circuit faults. The magnetizing current of transformer i_{Lm} is in continuous mode (CCM) with a low ripple to ensure that the ripple in output current I_o is minimised. Capacitor C_1 attenuates the ripple of the rectified voltage. Output capacitor C_o is a non-electrolytic capacitor, which reduces output flicker and prolongs the lifetime of the LED driver.

III. OPERATING MODES

Fig. 3 (a)-(d) demonstrates the equivalent circuits of the four main operating modes in the proposed LED driver. Meanwhile, Figs. 4 to 6 depict the idealized voltage and current waveforms of the proposed circuit based on those four modes of operation. The descriptions of operating modes in subsections III A-D refer to Figs. 3 to 6.

A. MODE I [$t_0 \le t < t_1$]

In Mode I, switch S_1 is turned on. Energy is transferred from the dc source and stored in inductor L_1 and the energy in capacitor C_1 is released to magnetizing inductor L_m and leakage inductor L_{lk}. Current in S_1 is the sum of current in L_1 and C_1 where,

$$i_{S_1}(t) = i_{L_1}(t) + i_{C_1}(t) = i_{L_1}(t) + i_{L_m}(t). \quad (1)$$

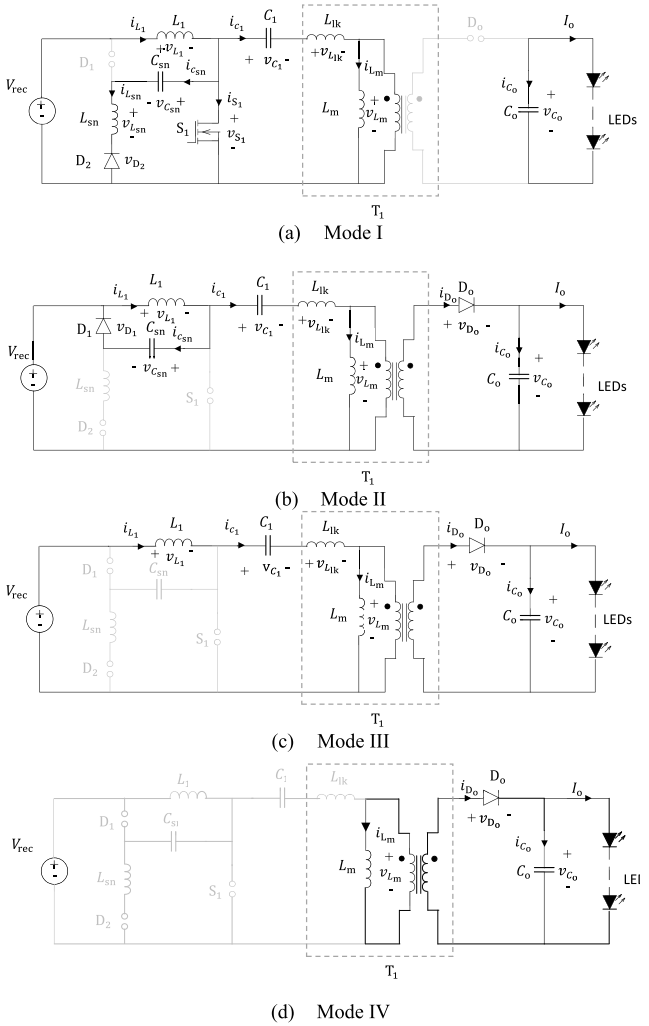

FIGURE 3. The main operating modes of the proposed LED driver.

No current flow in output diode D_o as it is reverse biased in Mode I. Therefore, output capacitor C_o supplies energy to the LED load. In the non-dissipative snubber, C_{sn} resonates with L_{sn} through the forward biased D_2.

B. MODE II [$t_1 \le t < t_2$]

Mode II begins when switch S_1 is turned off at $t = t_1$. The transformer magnetising inductor L_m, leakage inductance L_{lk} and capacitor C_1 discharge energy to snubber capacitor C_{sn} since L_{lk} resists the sudden change of current direction. As a result, the overvoltage in S_1 is minimized, thus increasing the reliability of the proposed LED driver. Energy in inductor L_1 is also discharged in C_{sn} via diode D_1. The duration for Mode II is very much shorter than the other operating modes due to the small value of C_{sn}. In this mode, the energy in the primary side of transformer T_1 is transferred to the secondary side to charge output capacitor C_o and to supply energy to the LEDs via diode D_o. Meanwhile, D_2 is reverse-biased.

C. MODE III [$t_2 \le t < t_3$]

Mode III begins when C_{sn} is fully-charged. At steady state, assuming that the effect of transformer leakage inductance is negligible, the peak voltage across S_1, V_{S_1} is expressed as,

$$v_{S_1} = V_{rec} + \frac{N_1}{N_2} V_o, \tag{2}$$

where $N_1/N_2 = 1$. From Fig. 4(a), i_{L1} decreases linearly to zero, where the current in L_1 is discontinuous. The dc input source and inductor L_1 transfer energy to capacitor C_1 and current flows in the primary winding of transformer T_1. Magnetizing inductance L_m discharges its energy into the primary winding of T_1. Diode D_o is forward biased, which provides a conducting path for the secondary winding of T_1 to transfer the energy to C_o and LEDs.

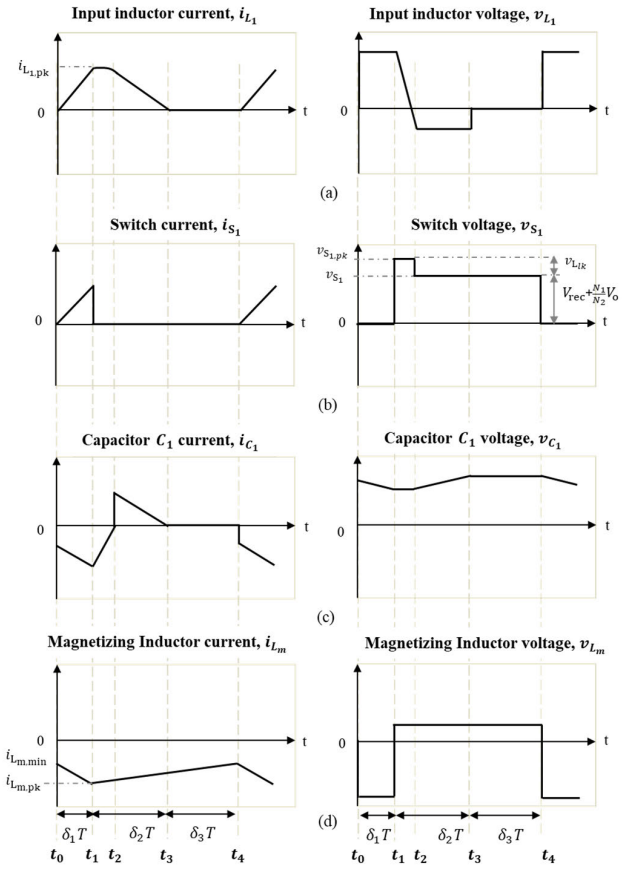

FIGURE 4. Idealized current and voltage waveforms in the primary side components of the proposed LED driver. (a) Input inductor L_1. (b) Switch S_1. (c) Storage capacitor C_1. (d) Magnetizing inductor L_m.

D. MODE IV [$t_3 \le t < t_4$]

Mode IV begins when inductor current $i_{L1} = 0$. Since L_1 operates in DCM while L_m operates in CCM, the value for inductor L_m is much larger than L_1. Therefore, energy from L_m is transferred to the LEDs through output diode D_o. When capacitor C_1 is fully charged, it blocks any current flow through it. The current in the magnetizing inductance is equal to the current in the primary winding

of T_1. Moreover, snubber diodes, D_1 and D_2 are reverse biased. Thus, no current flow in C_{sn} and L_{sn}.

IV. MODEL DESIGN

A. INPUT INDUCTOR L_1

Input inductor L_1 has discontinuous mode of operation ensuring that the ac source current is in phase with the ac source voltage, given that switch S_1 is operated at a constant switching frequency and duty cycle. As a result, the power factor is high without requiring any PFC circuit or a feedback controller. From Fig. 4(a), the discontinuous operation begins when i_{L_1} becomes zero at $t = t_3$.

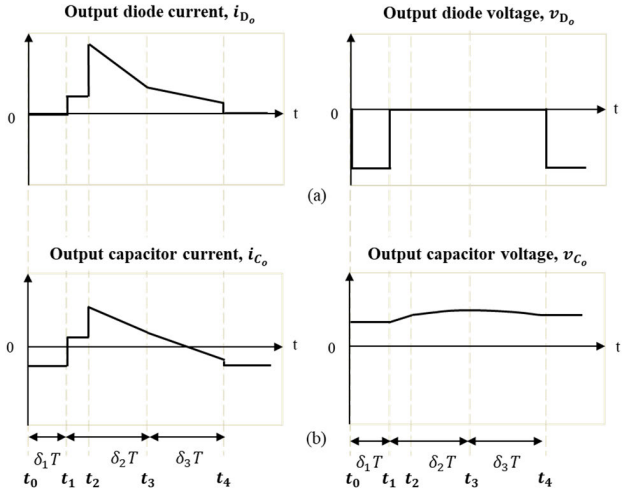

FIGURE 5. Idealized current and voltage waveforms in the secondary side components of the proposed LED driver. (a) Output diode D_O. (b) Output capacitor C_O.

In the first approximation, inductor L_1 is designed to realize boundary conduction mode and the isolated SEPIC is assumed to be ideal. Therefore, the input power P_{in} is equal to the output power P_{out} and the equality is expressed as,

$$V_{rec}.I_{L_1} = \frac{V_o^2}{R_e}, \tag{3}$$

where V_{rec} is assumed to be the average output voltage of a single-phase full-wave uncontrolled rectifier, I_{L_1} is the average input inductor current, V_o is the average output voltage and R_e is the static equivalent resistance of the modelled LEDs. The average output voltage of the diode rectifier is expressed as,

$$V_{rec} = \frac{2V_m}{\pi}, \tag{4}$$

where V_m is the maximum ac input voltage, while the average input inductor current I_{L_1} is determine from Fig. 4(a) as,

$$\begin{aligned} I_{L_1} &= \frac{1}{T}\left[\int_{t_0}^{t_1} \frac{i_{L_{1,pk}} t}{\delta_1 T} dt + \int_{t_2}^{t_3} \left(\frac{-i_{L_{1,pk}} t}{\delta_2 T} + i_{L_{1,pk}}\right)\right] dt, \\ &= \frac{1}{T}\left[\frac{i_{L_{1,pk}}}{\delta_1 T}.\frac{t^2}{2}\right]_{t_0}^{t_1} + \frac{-i_{L_{1,pk}}}{\delta_2 T}.\frac{t^2}{2}\Big]_{t_2}^{t_3} + i_{L_{1,pk}} t\Big]_{t_2}^{t_3}\Bigg], \\ &= \frac{i_{L_{1,pk}}}{T}\left[\frac{(\delta_1 T)^2}{2\delta_1 T} - \frac{(\delta_2 T)^2}{2\delta_2 T} + \delta_2 T\right], \\ &= \frac{i_{L_{1,pk}}}{2}(\delta_1 + \delta_2), \\ &= \frac{\Delta i_{L_1}}{2}(\delta_1 + \delta_2), \end{aligned} \tag{5}$$

where δ_1 and δ_2 are the durations for Modes I and III (the duration of Mode II is assumed to be negligible) and T is the switching period. The change in input inductor current Δi_{L_1} can be expressed as

$$\Delta i_{L_1} = \frac{\left(\frac{N_1}{N_2}\right) V_o \delta_2 T}{L_1}. \tag{6}$$

By substituting (6) into (5), the average input inductor current I_{L_1} is

$$I_{L_1} = \frac{\left(\frac{N_1}{N_2}\right) V_o \delta_2 T\,(\delta_1 + \delta_2)}{2L_1}. \tag{7}$$

When substituting (4) and (7) into (3), the input and output power equality can be rewritten as

$$\left(\frac{2V_m}{\pi}\right)\left(\frac{\left(\frac{N_1}{N_2}\right) V_o \delta_2 T\,(\delta_1 + \delta_2)}{2L_1}\right) = \frac{V_o^2}{R_e}. \tag{8}$$

Therefore, the input inductor L_1 is determined as,

$$L_1 = \frac{V_m \delta_2 T R_e\,(\delta_1 + \delta_2)}{\left(\frac{N_2}{N_1}\right) V_o \pi}. \tag{9}$$

During the boundary conduction mode, $\delta_1 = (1 - \delta_2)$. Therefore, for current i_{L1} to be discontinuous, the input inductor L_1 should be

$$L_1 < \frac{V_m T R_e (1 - \delta_1)}{\left(\frac{N_2}{N_1}\right) V_o \pi}. \tag{10}$$

In DCM operation, $\delta_1 + \delta_2 \neq 1$.

B. MAGNETIZING INDUCTOR L_m

The output current ripple, ΔI_o is proportional to the current ripple present in the magnetizing inductor of the transformer. Therefore, the transformer is designed to operate in continuous mode and low magnetizing inductor current ripple to ensure a smaller output current ripple and a smaller output capacitor C_o. When switch S_1 is turned off, the magnetizing inductor current is expressed as

$$i_{L_m} = i_{C_1} - \frac{N_2}{N_1} i_{D_o}. \tag{11}$$

On the secondary side, the diode current is expressed as,

$$i_{D_o} = i_{C_o} + I_o. \tag{12}$$

By substituting (12) into (11), the magnetizing inductor current i_{L_m} is rewritten as,

$$i_{L_m} = i_{C_1} - \frac{N_2}{N_1}\left(i_{C_o} + I_o\right). \tag{13}$$

In steady state, the average capacitor currents of C_1 and C_o are zero. Therefore, the average magnetizing inductor current is

$$I_{L_m} = \left| \frac{N_2}{N_1} I_o \right|. \tag{14}$$

Continuous current operation requires that the minimum magnetizing inductor current $i_{L_{m,min}} > 0$. At the boundary of CCM and DCM, $i_{L_{m,min}} = 0$. Therefore,

$$\frac{\Delta i_{L_m}}{2} - I_{L_m} = 0. \tag{15}$$

When switch S_1 is turned on,

$$v_{C_1} + v_{L_m} = 0, \tag{16}$$

Since the average voltage of capacitor C_1 is V_{rec}, the voltage across magnetizing inductor when S_l turned on is

$$v_{L_m} = -\frac{2V_m}{\pi}. \tag{17}$$

Therefore, the change in magnetizing inductor current is expressed as

$$\Delta i_{L_m} = -\frac{2V_m \delta_1 T}{\pi L_m}. \tag{18}$$

Substituting (14) and (18) into (15),

$$\frac{V_m \delta_1 T}{\pi L_m} - \frac{N_2}{N_1} I_o = 0. \tag{19}$$

In order for the magnetizing current to be CCM, the magnetizing inductance should be larger than the minimum magnetizing inductor from (14), therefore

$$L_m > \frac{V_m \delta_1 T N_1}{N_2 \pi I_o}. \tag{20}$$

C. STORAGE CAPACITOR C_1

When switch S_1 turns on, the change in charge of C_1 is expressed as

$$\left|\Delta Q_{C_1}\right| = \frac{1}{2}\left(i_{L_{m,min}} + i_{L_{m,pk}}\right)\delta_1 T. \tag{21}$$

The minimum and maximum current of magnetizing inductor $i_{L_{m,min}}$ and $i_{L_{m,pk}}$ are expressed as

$$i_{L_{m,min}} = \frac{N_2}{N_1} I_o + \frac{V_m \delta_1 T}{\pi L_m}, \tag{22}$$

$$i_{L_{m,pk}} = \frac{N_2}{N_1} I_o - \frac{V_m \delta_1 T}{\pi L_m}. \tag{23}$$

By substituting (22) and (23) into (21), the change in charge of capacitor C_1 is

$$\Delta Q_{C_1} = \frac{N_2}{N_1} I_o \delta_1 T. \tag{24}$$

The value of storage capacitor C_1 is expressed as the change in charge per unit in capacitor voltage,

$$C_1 = \frac{\Delta Q_{C_1}}{\Delta v_{C_1}}. \tag{25}$$

When substituting (24) into (25),

$$C_1 = \frac{N_2 I_o \delta_1 T}{N_1 \Delta v_{C_1}}. \tag{26}$$

The average output current $I_o = V_o/R_e$. Therefore, the storage capacitor C_1 is

$$C_1 = \frac{N_2 \delta_1 T}{N_1 R_e \left(\Delta v_{C_1}/V_o\right)}. \tag{27}$$

When switch S_1 turns off,

$$V_{rec} = v_{L_1} + v_{C_1} + \left(v_{L_{lk}} + v_{L_m}\right). \tag{28}$$

Since the average voltage across the inductors are zero, therefore the average voltage of storage capacitor C_1 is,

$$V_{C_1} = \frac{2V_m}{\pi}. \tag{29}$$

The ratio of change in voltage with average voltage of C_1 is expressed as,

$$v_{C_{1,ripple}} = \frac{\Delta v_{C_1}}{V_{C_1}}. \tag{30}$$

Substituting (29) and (30) into (27), the value of capacitor C_1 is,

$$C_1 = \frac{N_2 \delta_1 T}{N_1 R_e \left(v_{C_{1,ripple}} 2V_m/\pi V_o\right)}. \tag{31}$$

D. OUTPUT CAPACITOR C_o

When switch S_1 turns on, the voltage across the output capacitor C_o is the same as the output voltage V_o with ripple of double the line frequency ($f_l = 100$Hz). The change of charge in capacitor C_o can be expressed as

$$\left|\Delta Q_{C_o}\right| = C_o \Delta V_{C_o} = \frac{V_o}{R_e}\delta_1 T_l. \tag{32}$$

where T_l is double the line period with a value of 10ms. Rearranging (32), the expression for the output capacitor C_o is,

$$C_o = \frac{V_o \delta_1 T_l}{\Delta V_o R_e}. \tag{33}$$

E. NON-DISSIPATIVE SNUBBER DESIGN

The peak voltage of S_1, $v_{S_{1,pk}}$ as shown in Fig. 4(b) is limited below the breakdown voltage of S_1 [13]

$$v_{S_{1,pk}} = v_{S_1} + i_{L_{lk}}\sqrt{L_{lk}}/C_{sn}, \tag{34}$$

where v_{S_1} is calculated as (2). Therefore, the value of the snubber capacitor C_{sn} of the proposed converter is

$$C_{sn} = \frac{I_{L_1}^2 L_{lk}}{\left[v_{S_{1,pk}} - \left(\frac{2V_m}{\pi}\right) - \left(\frac{N_2}{N_1}\right) V_o\right]^2}. \tag{35}$$

To prevent energy backflow into the source side during switch turn on, snubber capacitor C_{sn} and inductor L_{sn} shall not resonate so that the direction of current does not change

and D_1 remains reverse-biased. Therefore, the maximum value of $-v_{C_{sn,pk}}$ must be lower than rectified voltage $V_{rec} = \frac{2V_m}{\pi}$. This limitation can be used to derive the value for L_{sn} as the following

$$I_{C_{sn,pk}} = v_{C_{sn,pk}}\sqrt{C_{sn}}/L_{sn}, \tag{36}$$

$$L_{sn} = \frac{V_{rec}^2 C_{sn}}{I_{C_{sn,pk}}^2}, \tag{37}$$

Note that the switch turn-on time T_{on} is also constraint as [13],

$$T_{on} \geq \pi\sqrt{L_{sn}C_{sn}} \tag{38}$$

in order to ensure no back flow of current into the source.

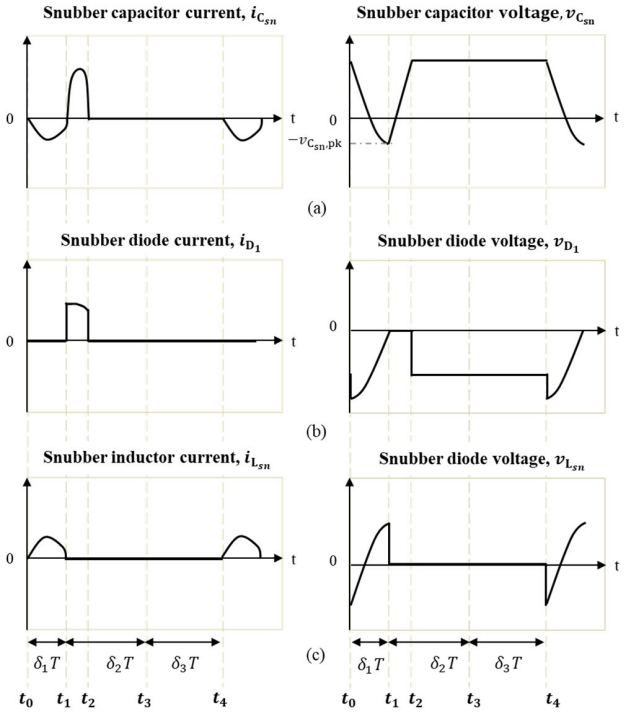

FIGURE 6. Idealized current and voltage waveforms in the snubber. (a) Snubber capacitor C_{sn}. (b) Snubber diode, D_1. (c) Snubber inductor L_{sn}.

V. SIMULATION AND EXPERIMENTAL VERIFICATION

A. SIMULATION RESULTS AT THE INPUT VOLTAGE OF 240V

Fig. 7 presents the proposed LED driver that is modelled in Simulink®. The LED driver consists of an EMI filter, a front-end diode rectifier, a non-dissipative DRS snubber and an isolated SEPIC. The LED driver is connected to a single-phase 50Hz ac voltage supply, v_s, that is varied between 90V and 240V to emulate a universal input. An inductor-capacitor L_fC_f filter is connected at the ac input of the diode rectifier to reduce harmonics in the ac current i_s. The diode rectifier converts ac voltage to an unregulated dc voltage. The average output voltage of the diode rectifier, V_{rec} provides input voltage to the primary side of the isolated SEPIC.

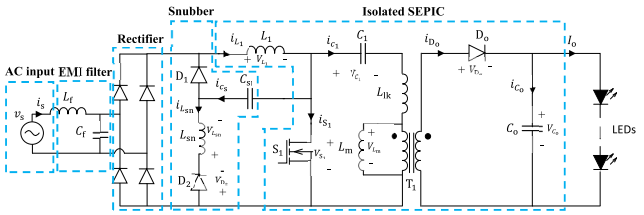

FIGURE 7. The electrical circuit of the proposed LED driver.

TABLE 1. Circuit parameters of the proposed led driver.

Component	Symbol	Value	Unit
Input line voltage	v_s	90-240	V
Total forward voltage of LED	V_o	30	V
LED current	I_o	0.6	A
Rated output power	P_o	18	W
Duty ratio	δ	0.08-0.21	-
Equivalent resistor	R_e	50	Ω
Switching frequency	f_{sw}	60	kHz
Input inductor	L_1	190	μH
Filter inductor	L_f	2	mH
Filter capacitor	C_f	33	nF
Snubber inductor	L_{sn}	50	μH
Snubber capacitor	C_{sn}	1	μF
Snubber and output diodes	D_1, D_2, D_o	-	-
Storage capacitor	C_1	6.6	μF
Transformer	T_1	N_2/N_1 =1:1	
Output capacitor	C_o	88	μF

Table 1 presents the values of the circuit parameters employed in the proposed LED driver. An array of 9-by-4 3.3-V 1-W LEDs are connected to the output of the isolated SEPIC. The current in the LED array is designed to be 150 mA in each string at the rated power of 18W. No control of brightness has been considered in this study.

Fig.8 presents the simulated ac input current and voltage waveforms of the proposed LED driver at input voltage 240V and the rated output power of 18W. The peak of ac input voltage is 339V while the peak of ac input current is 0.2A. An FFT analyser tool in Simulink® is used to measure the harmonics level in the input current. Fig. 9 shows that the harmonics levels in the simulated LED driver are less than the allowable limits in the IEC 61000-3-2 Class C standard.

The power factor of the proposed LED driver is measured by taking the ratio of load active power and source apparent power. The power factor obtained for the proposed LED driver at input voltage 240V is 0.92 which complies with the Energy Star standard that specifies the power factor of LED drivers to be higher than 0.9 for commercial LED light and 0.7 for residential LED light.

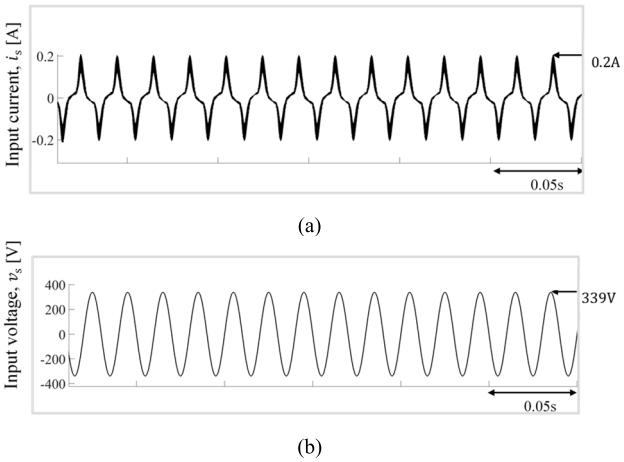

FIGURE 8. Simulation waveforms of ac current and voltage when the applied input voltage is 240V_{RMS} and the rated output power is 18W. (a) Input current, i_S and (b) Input voltage, v_S.

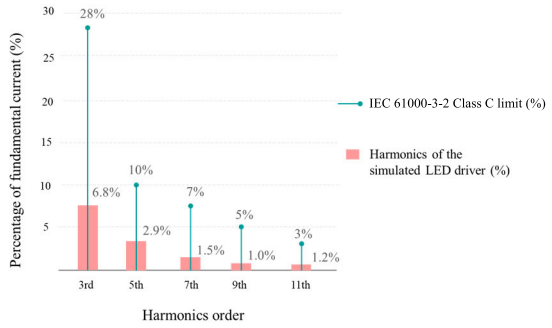

FIGURE 9. Comparison of the harmonics current level obtained in the simulation model of the proposed LED driver with the IEC-61000-3-2 Class C standard.

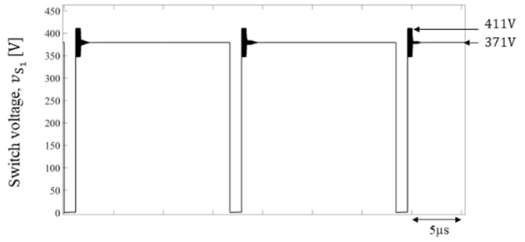

FIGURE 10. Simulation waveform of switch voltage v_{S1} of the isolated SEPIC model with non-dissipative snubber DRS when the ac input voltage is 240V and the rated output power is 18W.

Fig. 10 shows the simulation voltage waveform of switch S_1, v_{S1}, when the applied input AC voltage is 240V and the rated output power is 18W. At steady-state, the turn-off voltage of S_1 is 371V. The maximum transient voltage is 411V. The transient overvoltage is 40V. A MOSFET rating between 600V and 900V can be selected for the experimental prototype.

B. EXPERIMENTAL RESULTS AT 240V INPUT

Fig. 11 presents the photo of the experimental setup of the proposed 30-V 18-W LED driver. A 50Hz, 90-240V variable

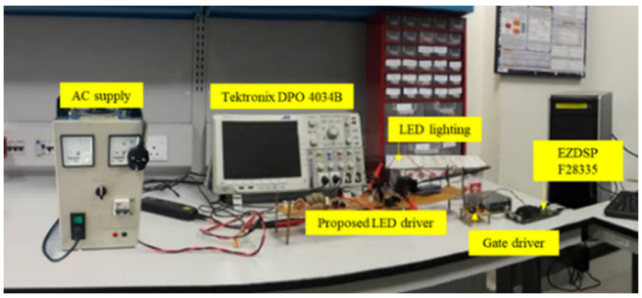

FIGURE 11. The photo of the experimental setup.

ac voltage supply is connected at the input of the LED driver. A digital signal processor is used to generate PWM signals between 0 and 3.3V, which are amplified between 0 and 15V by a gate driver. In order to maintain the output voltage of the LED driver at 30V when the input voltage varies between 90 and 240V, the duty cycle of the switch in the isolated SEPIC is varied between 0.07 and 0.21. Note that, the overall system of the prototype circuit is not optimized in terms of its size and arrangement. Table 2 shows the model and rating of components used in the LED driver prototype.

TABLE 2. Components model and rating.

Component	Symbol	Model Part	Rating
Diode rectifier	-	4 x 1N5408	Repetitive peak reverse voltage, V_{RRM}=1kV
Input inductor	L_1	-	1.5A
Snubber inductor	L_{sn}	-	1A
Snubber capacitor	C_{sn}	ECW-HA3C102JB	V_{RRM}=1.6kV
Snubber and output diode	D_1, D_2, D_o	STTH3010D	V_{RRM}=1kV
Switch	S_1	STW12NK90Z	Drain-source voltage, V_{DS}=900V
Storage capacitor	C_1	2 x F611DU335M400	Rated DC voltage=400V
Output capacitor	C_o	4 x R60DR5220AA40K	Rated DC voltage=63V

Fig. 12 shows the measured waveforms of the ac current i_s and ac voltage v_s when the input voltage is 240V and the rated output power is 18W. The peak input current is 0.21A and the peak input voltage is 339V. The measured power factor is 0.924. Fig. 13 illustrates the measured power factor when the ac input voltage is varied from 90 to 240V. The results show that the proposed LED driver has power factor more than 0.9 within the universal input voltage range. The power factor complies with Energy Star guidance for commercial use.

Fig. 14 compares the measured ac input current harmonics with the limits set in IEC-6100-3-2 Class C standard.

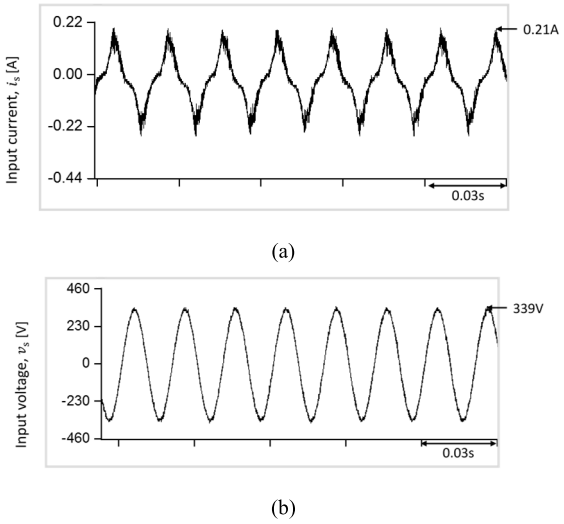

FIGURE 12. Experimental waveforms of ac current and voltage. (a) Input current i_s. (b) Input voltage v_s.

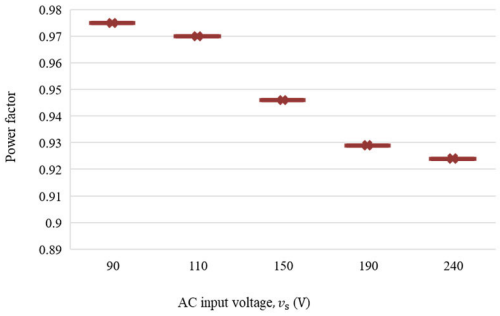

FIGURE 13. Measured power factor of the proposed LED driver when the input voltage is varied from 90 to 240V at the rated power of 18W.

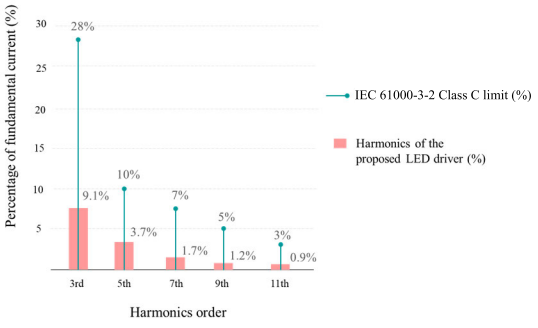

FIGURE 14. Comparison of measured ac harmonic current level with the IEC-61000-3-2 Class C standard.

The ac input current harmonics are measured using the analyzer function in digital phosphor oscilloscope Tektronix DPO4034B. It can be seen that harmonic contents from the proposed LED driver are lower than the set limits. Both the power factor and harmonics results show that the proposed LED driver has a good power quality.

Fig. 15 shows the measured voltage waveform of switch S_1, v_{S1}, when the input voltage 240V and the rated output power is 18W. Since the DRS snubber is employed, the maximum transient voltage is 480V and the steady-state voltage is 414V.

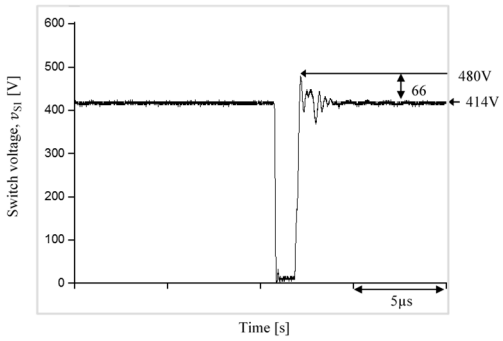

FIGURE 15. Switch voltage v_{s1} of the isolated SEPIC with the non-dissipative DRS snubber when the ac input voltage is 240V and the rated output power is 18W.

TABLE 3. Comparison between simulation and experimental results at the rated operating condition of 240V_{rms} and 18W.

	SIMULATION	EXPERIMENT
Peak Input Current (A)	0.2	0.21
Power Factor	0.92	0.924
Odd Harmonics Value		
3^{rd}	6.8%	9.1%
5^{th}	2.9%	3.7%
7^{th}	1.5%	1.7%
9^{th}	1.0%	1.2%
11^{th}	1.2%	0.9%
Average Output Current (A)	0.6	0.6
Average Output Voltage(V)	30	30
Peak Switch Voltage (V)	411	480
Steady-state Voltage (V)	371	414

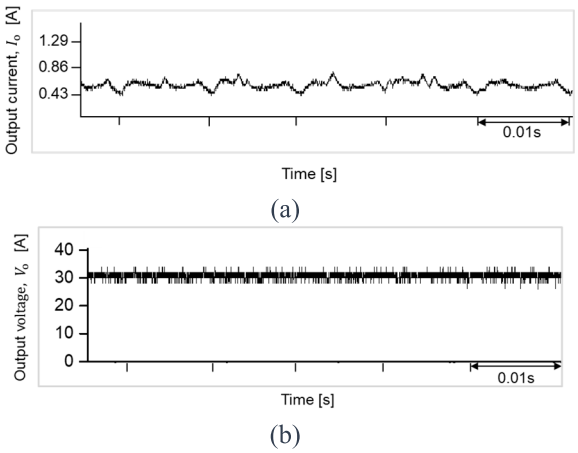

FIGURE 16. Dc current and voltage waveforms at the ac input voltage of 240V and the rated output power of 18W. a) Output current i_o. b) Output voltage v_o.

Fig. 16 presents the dc output voltage and current waveforms of the 18W LED lighting. The average output voltage is 30V and the average output current is 0.6A. The current of the18W LED array has a flicker of 29% at 100Hz.

The flicker value of the 18W LED array is relatively high. However, it complies with the limit in CEC Title 24 JA8 standard. The output current ripple can be further reduced by increasing the value of output capacitor, C_o. If lifetime of the LED driver is to be lengthen, then a film capacitor should be used because it has a longer lifetime limit than an electrolytic capacitor. However, the footprint of the output capacitor may increase. Therefore, there should be a trade-off in the LED driver design.

Table 3 compares the simulation and experimental results of the proposed LED driver when the ac input voltage is 240V and the rated output power is 18W. The peak input current and power factor in the simulation and experimental circuits agree with each other, while certain odd harmonics in the simulation circuit is slightly lower than in the experimental prototype. Power factor and harmonics current levels meet the Energy Star guidelines and the IEC 61000-3-2 Class C standard, respectively. The maximum voltage and steady-state voltage during switch turn-off are higher in the experimental circuit, which could be caused by parasitic inductances that exist in the experimental circuit that was not modelled in simulation. The results from the simulation model and the experimental setup are similar.

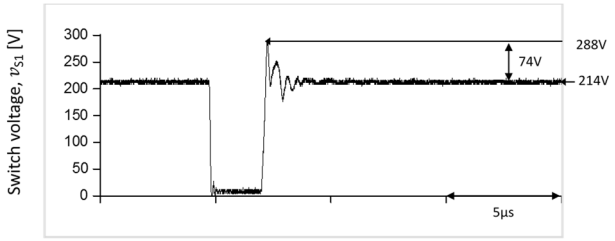

FIGURE 17. Switch voltage v_{s1} of the isolated SEPIC with non-dissipative DRS snubber at ac input voltage 110V and rated output power of 18W.

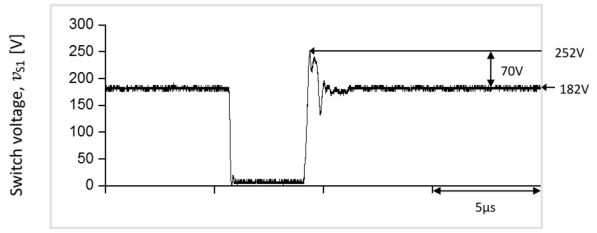

FIGURE 18. Switch voltage v_{s1} of the isolated SEPIC with non-dissipative DRS snubber at ac input voltage 90V and rated output power of 18W.

C. SWITCHING OVERVOLTAGE REVIEW

Figs. 17 to 19 shows the switching voltage waveforms of the proposed LED driver with various ac input voltages. The measured steady state voltages of switch S_1 are 182, 214 and 286V when the ac input voltages are 90, 110, and 150V respectively. The maximum voltage in S_1 due to the over voltage ringing is 252, 288 and 368V as the ac voltage increases.

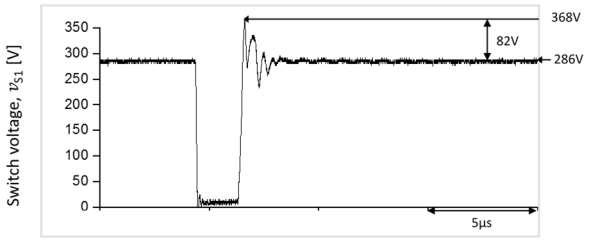

FIGURE 19. Switch voltage v_{s1} of the isolated SEPIC with non-dissipative DRS snubber at ac input voltage 150V and rated output power of 18W.

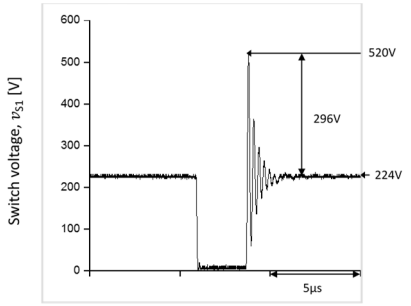

FIGURE 20. Switch voltage, v_{s1} of the isolated SEPIC without snubber at ac input voltage 110V and rated output power of 18W.

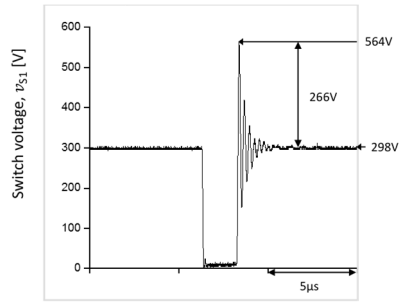

FIGURE 21. Switch voltage, v_{s1} of the isolated SEPIC without snubber at ac input voltage 150V and rated output power of 18W.

TABLE 4. Comparison of switch S_1 voltage in the isolated sepic circuit with and without the non-dissipative drs snubber.

	Maximum voltage $V_{S_{1max}}$ [V]			Steady state voltage V_{S_1} [V]			Overvoltage $(V_{S_{1max}} - V_{S_1})$ [V]		
Input voltage, v_s	**90**	**110**	**150**	**90**	**110**	**150**	**90**	**110**	**150**
Isolated SEPIC with snubber	252	288	368	182	214	286	70	74	82
Isolated SEPIC without snubber	472	520	564	186	224	298	286	296	266

Figs. 20 and 21 present the switching voltage waveforms of the prototype without the non-dissipative DRS snubber. The ac input voltage is supplied at the same voltage of 110 and 150V. At steady-state, the voltage across S_1 is 224 and 298V as the ac input voltage increases. It can be seen from the figures that the maximum over voltage in the prototype is much higher without snubber. The maximum

TABLE 5. Comparison of the proposed led driver with other research work on isolated sepic converter with snubber.

	[16]	[4]	[17]	[18]	[19]	Proposed LED driver
Input Voltage (V)	22-32 Vac	185-220 Vac	42 Vdc	277 Vac	100 Vac	90-240 Vac
Output Voltage (V)	25.5	30	200	400	28	30
Output Power (W)	34	21	10-100	400-2000	300	18
Switching Frequency (kHz)	-	50	50	200	50	60
Output Capacitor (µF)	-	10	-	800	1360	88
Peak Efficiency	82.3% at 34W	95% at 16.8W	95.9% at 50W	96.56% at 1200W	93.5% at 300W	95% at 18W
Power Factor	0.98-0.99	0.99		0.99	0.99	0.93-0.975
Overvoltage (V)	150	No overvoltage at turn-off, however peak voltage is high	16	63. The voltage in the main and snubber switches are high.	20	82
Steady-state Voltage (V)	70 at 32V input voltage	600 at 220V input voltage	80	900	250	286 at 150V input voltage
Snubber Type	Passive	Passive	Passive	Active	Active	Passive
Snubber Component Count	1 capacitor and 1 diode	1 inductor, 2 diodes and 2 capacitors	1 couple inductor, 1 inductor, 1 diode and 1 capacitor	1 switch and 2 capacitors	1 switch and 1 capacitor	1 inductor, 2 diodes and 1 capacitor
Flicker (%)	18	25	-	-	-	29

voltage in S_1 due to the over voltage ringing is 520 and 564V as the ac voltage increases.

Table 4 summarizes the maximum voltage, overvoltage and the steady-stage voltage of the isolated SEPIC with and without the snubber circuit. The DRS snubber circuit provided the advantage of minimizing up to more than 100V of overvoltage in switch S_1 improving the reliability of the isolated SEPIC circuit.

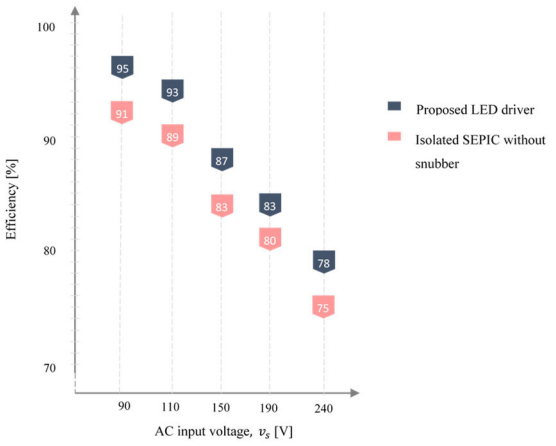

FIGURE 22. Efficiency of the proposed LED driver and the isolated SEPIC converter with and without snubber.

Fig. 22 presents the measured efficiency of the LED driver with and without the non-dissipative DRS snubber. The efficiency of the proposed LED driver is measured at different ac input voltage at the rated output power of 18W. The efficiency n is measured as,

$$n = \frac{P_{\text{in}}}{P_{\text{out}}}, \tag{39}$$

where $P_{\text{in}} = v_s i_s \cos\theta$ and $P_{\text{out}} = V_o I_o$. The efficiency of the proposed LED driver ranges from 78% to 95%. The proposed circuit with the non-dissipative snubber has around 3% to 4% higher efficiency than the circuit without the snubber because the non-dissipative snubber reduces switching losses in S_1 by minimizing the switch overvoltage. The efficiency range of the proposed converter is comparable to the range that has been reported, which is typically between 79 to 96% for an isolated SEPIC based on various input and output voltages [4], [5], [16]–[19]. The efficiency of the proposed LED driver can be further improved if the PCB circuit is optimized in terms of its connection and arrangement.

Table 5 compares the proposed LED driver with a range of isolated SEPIC converters that uses passive and active snubbers described in [4], [16]–[19]. The proposed LED driver is operated in universal input voltage range between 90V and 240V, achieves power factor of more than 0.9, peak efficiency of 95%, and uses a non-electrolytic output capacitor. There are very few published literatures that have tested the isolated SEPIC for LED application in universal input voltage. Moreover, the proposed non-dissipative DRS snubber reduces the switching overvoltage by more than 69% compared to isolated SEPIC without snubber as depicted in Table 4.

The LED driver in [16] has a high power factor that ranges from 0.98 to 0.99 and low output current ripple at only 18%. The type and value of output capacitor used has not been discussed. It utilizes a simple capacitor-diode (CD) snubber and is able to reduce 41% of the overvoltage during switch turn-off as compared to the isolated SEPIC converter without snubber application.

However, the overvoltage is double the steady state voltage, which required a large snubber capacitor. Therefore, the LED driver with the CD snubber is suitable for application with low

input voltages. The peak efficiency is low at 82.3% when the output power is 32W.

The circuit proposed in [4] has presented a 30-V, 21-W LED driver with the power factor of 0.99. The odd harmonics complies with the IEC 61000-3-2 Class C standard, flicker is 25% which satisfies the limit set by California Energy Commission (CEC) Title 24 JA8 standard, non-electrolytic capacitors are used and the peak efficiency is 95%. Even though spikes are not present during switch turn-off in [4], the voltage stress in the switch is relatively high because the constant turn-off voltage is triple the input voltage. There is a trade-off between the power factor and switching voltage where a lower voltage stress in the switch would decrease the power factor due to smaller value of the storage and snubber capacitors.

The dc-dc converter of [17] uses coupled-inductor, auxiliary capacitor, auxiliary inductor and diode to reduce the switch overvoltage as well as remove the ripple in the input current. The overvoltage is 20% of the steady state voltage and the efficiency is improved by 1.3% compared to the isolated SEPIC with conventional RCD snubber. However, the couple inductor increases the footprint of the converter and a larger turns ratio will cause a higher conduction loss.

The proposed LED driver is also compared to the isolated SEPIC converters in [18] and [19], which are employed in high power applications of up to 2kW and 300W, respectively. In both applications, active snubbers were employed. The LED drivers comply to the Energy Star standard for power factor, have efficiency more than 90%, and harmonics levels that comply with IEC 6100-3-2 Class C standard. The overvoltage in both LED drivers is low at 7% and 8% of the steady state voltage, respectively. However, the usage of active snubbers increases the complexity and cost while reducing the reliability of the LED drivers. Moreover, the voltage stress in [18] are high at the main and snubber switches.

VI. CONCLUSION

This paper has presented a detailed description and circuit design of a high-performance isolated SEPIC converter with a non-dissipative snubber for an LED driver. The input inductor L_1 of the proposed LED driver has been designed to operate in DCM to achieve a high-power factor. In addition, the magnetising inductor L_m of the transformer has been designed to operate in CCM to reduce ripple in the output current and voltage. With minimized output ripple voltage, the output capacitor C_o can be a non-electrolytic-type, which results in prolonging the lifetime of the LED driver. The step-by-step design equations of the inductors and capacitors in the isolated SEPIC and snubber circuits have been explained in this paper. The simulation and experimental results showed that the proposed converter has power factor more than 0.9, the current harmonics complied with IEC-61000-3-2 Class C standard and an efficiency that ranges between 78% and 95%. A DRS snubber is used to minimize the switching overvoltage and increase the reliability of the isolated SEPIC. The experimental results revealed that overvoltage of the switch is minimized and the efficiency is improved by 3% to 4% at different input voltages in the proposed LED driver as compared to the isolated SEPIC without the snubber.

REFERENCES

[1] *Lifetime and Reliability*, U.S. Department of Energy, Washington, DC, USA, 2014, p. 3.
[2] M. Brown, *Power Supply Cookbook*, Newnes, Boston, MA, USA, 2001.
[3] G. Tibola, E. Lemmen, J. L. Duarte, and I. Barbi, "Passive regenerative and dissipative snubber cells for isolated SEPIC converters: Analysis, design, and comparison," *IEEE Trans. Power Electron.*, vol. 32, no. 12, pp. 9210–9222, Dec. 2017.
[4] B. Poorali and E. Adib, "Analysis of the integrated SEPIC-flyback converter as a single-stage single-switch power-factor-correction LED driver," *IEEE Trans. Ind. Electron.*, vol. 63, no. 6, pp. 3562–3570, Jun. 2016.
[5] Z. Liao, H. Gu, C. Cao, and Z. Chen, "Research on a single-stage isolated electrolytic capacitor-less LED driver," *Optik*, vol. 225, Jan. 2021, Art. no. 165688.
[6] P. Fang, Y.-J. Qiu, H. Wang, and Y.-F. Liu, "A single-stage primary-side-controlled off-line flyback LED driver with ripple cancellation," *IEEE Trans. Power Electron.*, vol. 32, no. 6, pp. 4700–4715, Jun. 2017.
[7] G. M. Soares, J. M. Alonso, and H. A. C. Braga, "Investigation of the active ripple compensation technique to reduce bulk capacitance in offline flyback-based LED drivers," *IEEE Trans. Power Electron.*, vol. 33, no. 6, pp. 5206–5214, Jun. 2018.
[8] P. Fang, S. Webb, Y.-F. Liu, and P. C. Sen, "Single-stage LED driver achieves electrolytic capacitor-less and flicker-free operation with unidirectional current compensator," *IEEE Trans. Power Electron.*, vol. 34, no. 7, pp. 6760–6776, Jul. 2019.
[9] I. Castro, K. Martin, A. Vazquez, M. Arias, D. G. Lamar, and J. Sebastian, "An AC–DC PFC single-stage dual inductor current-fed push–pull for HB-LED lighting applications," *IEEE J. Emerg. Sel. Topics Power Electron.*, vol. 6, no. 1, pp. 255–266, Mar. 2018.
[10] A. Malschitzky, E. Agostini, and C. B. Nascimento, "Integrated bridgeless-boost nonresonant half-bridge converter employing hybrid modulation strategy for LED driver applications," *IEEE Trans. Ind. Electron.*, vol. 68, no. 9, pp. 8049–8060, Sep. 2021.
[11] V. K. S. Veeramallu, S. Porpandiselvi, and B. L. Narasimharaju, "A nonisolated wide input series resonant converter for automotive LED lighting system," *IEEE Trans. Power Electron.*, vol. 36, no. 5, pp. 5686–5699, May 2021.
[12] S. Liu, H. Lin, and T. Wang, "Comparative study of three different passive snubber circuits for SiC power MOSFETs," in *Proc. IEEE Appl. Power Electron. Conf. Expo. (APEC)*, Mar. 2019, pp. 354–358.
[13] M. Domb, R. Redl, and N. Sokal, "Nondissipative turn-off snubber alleviates switching power dissipation, second-breakdown stress and VCE overshoot: Analysis, design procedure and experimental verification," in *Proc. IEEE Power Electron. Spec. Conf.*, Jun. 1982, pp. 445–454.
[14] M. L. Nadia Tan and S. N. D. Ahmad, "Non-dissipative isolated SEPIC converter for LED driver," U.S. Patent I2019 006 975, Nov. 27, 2019.
[15] Z. Ye, F. Greenfeld, and Z. Liang, "A topology study of single-phase offline AC/DC converters for high brightness white LED lighting with power factor pre-regulation and brightness dimmable," in *Proc. 34th Annu. Conf. IEEE Ind. Electron.*, Nov. 2008, pp. 1961–1967.
[16] P. R. R. Somarowthu, S. K. Saxena, and D. B. Mahajan, "Isolated SEPIC converter with a novel voltage clamp circuit," in *Proc. IEEE Int. Conf. Power Electron., Drives Energy Syst. (PEDES)*, Dec. 2018, pp. 1–6.
[17] S.-W. Lee and H.-L. Do, "Isolated SEPIC DC–DC converter with ripple-free input current and lossless snubber," *IEEE Trans. Ind. Electron.*, vol. 65, no. 2, pp. 1254–1262, Feb. 2018.
[18] D. Wu, R. Ayyanar, M. Sondharangalla, and T. Meyers, "High-performance active-clamped isolated SEPIC PFC converter with SiC devices and lossless diode clamp," *IEEE J. Emerg. Sel. Topics Power Electron.*, vol. 8, no. 1, pp. 567–577, Mar. 2020.
[19] W. Y. Choi and M. K. Yang, "High-efficiency isolated SEPIC converter with reduced conduction losses for LED displays," *Int. J. Electron.*, no. 11, pp. 1495–1502, 2014.

SULAIHA AHMAD received the B.S. and M.S. degrees in electrical engineering from Universiti Tenaga Nasional, Malaysia, in 2015 and 2020, respectively. She is currently doing a research on smart grid development at the Institute of Energy Policy and Research (IEPRe), Malaysia. Her research interests include ac/dc power converter, soft-switching power converter, smart grid, and LED lighting.

NADIA MEI LIN TAN (Senior Member, IEEE) was born in Kuala Lumpur, Malaysia. She received the B.Eng. (Hons.) degree in electrical engineering from The University of Sheffield, Sheffield, U.K., in 2002, the M.Eng. degree in electrical engineering from Universiti Tenaga Nasional, Kajang, Malaysia, in 2007, and the Ph.D. degree in electrical and electronic engineering from Tokyo Institute of Technology, Tokyo, Japan, in 2010.

From July 2016 to September 2016, she was an Adjunct Associate Professor at the Tokyo Institute of Technology. From October 2016 to March 2017, she was a Visiting Researcher with the Power Electronics Laboratory, Tokyo Institute of Technology. She has been an Associate Professor with the Department of Electrical and Electronics Engineering, Universiti Tenaga Nasional, since 2017. She is currently an Associate Professor at the Department of Electrical and Electronics Engineering, University of Nottingham Ningbo China. Her research interests include power conversion systems for renewable energy, battery energy storage applications, and bidirectional isolated dc–dc converters.

Dr. Tan is a Chartered Engineer registered with Engineering Council, U.K., a Professional Engineer registered with the Board of Engineers Malaysia, and a member of the Institution of Engineering and Technology and the Institution of Engineers Malaysia. She was a recipient of the 2018 IET Malaysia Network Young Engineer Award and the 2018 IPCC IEEE IAS Prize Paper Award. She has served as the Vice Chair for the IEEE Power Electronics Society Malaysia Chapter, from 2018 to 2019.

M. ZAFRI BAHARUDDIN (Member, IEEE) received the B.Eng. degree (Hons.) in electrical and electronics engineering from Universiti Tenaga Nasional, in 2004, the master's degree in electrical (mechatronics) engineering from Universiti Teknologi Malaysia, in 2008, and the Ph.D. degree in synthetic aperture radar from Chiba University, Japan.

He is currently lecturing on digital signal processing, robotics, and artificial intelligence at Universiti Tenaga Nasional, where he also performs research and consultancy in the same fields.

GIAMPAOLO BUTICCHI (Senior Member, IEEE) received the master's degree in electronic engineering and the Ph.D. degree in information technologies from the University of Parma, Italy, in 2009 and 2013, respectively.

In 2012, he was a Visiting Researcher at the University of Nottingham, U.K. From 2014 to 2017, he was a Postdoctoral Researcher and a Guest Professor at the University of Kiel, Germany. In 2017, he was appointed as an Associate Professor in electrical engineering at the University of Nottingham Ningbo China and the Head of the Power Electronics of the Nottingham Electrification Center. He was promoted to a Professor, in 2020. He is author/coauthor of more than 230 scientific papers. His research interests include power electronics for renewable energy systems, smart transformer fed micro-grids, and dc grids for the more electric aircraft. He is one of the advocates for DC distribution systems and multi-port power electronics onboard the future aircraft.

Dr. Buticchi is the Chair of the IEEE-IES Technical Committee on Renewable Energy Systems and the IES Energy Cluster Delegate. During his stay in Germany, he was awarded with the Von Humboldt Postdoctoral Fellowship to carry out research related to fault tolerant topologies of smart transformers. He is an Associate Editor of the IEEE TRANSACTIONS ON INDUSTRIAL ELECTRONICS, the IEEE TRANSACTIONS ON TRANSPORTATION ELECTRIFICATION, and the IEEE OPEN JOURNAL OF THE INDUSTRIAL ELECTRONICS SOCIETY.